Brackish springs in coastal aquifers and the role of calcite dissolution by mixing waters

Esteban Sanz Escudé

October 19, 2007

CHAPTER 5: CALCITE DISSOLUTION BY MIXING WATERS: NUMERICAL MODELING AND FLOW-TROUGH EXPERIMENTS

PhD Thesis
Department of Geotechnical Engineering and Geo-Sciences (ETCG)
Technical University of Catalonia (UPC)

Supervisors:
Dr. Jesús Carrera Ramírez
Dr. Carlos Ayora Ibáñez

Institute of Earth Sciences 'Jaume Almera', CSIC

Chapter 5

Calcite dissolution by mixing waters: numerical modeling and flow trough experiments

Mixing of calcite-saturated waters may lead to undersaturated solutions thus having a potential for calcite dissolution. This phenomenon can be caused by the superposition of several effects, being the algebraic, salinity, pCO_2 (together with pH), and temperature effects the most relevant (Wigley and Plummer, 1976). The algebraic effect refers to the non-linearity of the ion activity product with respect to the variation of total species concentrations, which vary linearly with mixing ratios. This causes oversaturation of mixtures, even if end members are in equilibrium, because the IAP of any linear mixture is always higher than Keq (Figure 5.1a).

The salinity effect (also called Ionic strength effect) occurs when two solutions having different salinity are mixed together. The resulting solution is subsaturated in calcite, as a consequence of the non-linear dependence of the ion activity coefficients with Ionic strength at low to moderate ion strength. This causes solubility of a mixture to be higher than the linear combination of the end member solutions, thus leading to undersaturation (Figure 5.1b).

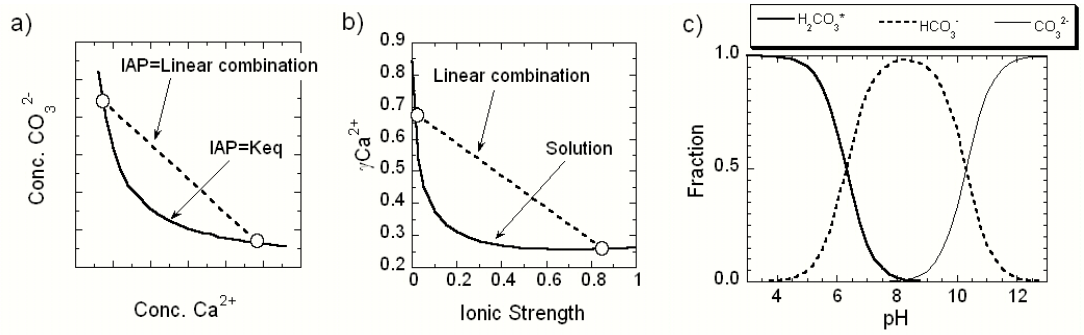

Figure 5.1: Factors affecting calcite saturation of a mixture of two calcite-saturated solutions: a) the algebraic effect: any linear combination of ions (IAP) is higher than Keq, therefore supersaturated; b) the salinity effect: the ion activity for ions in solution is smaller than that of the linear combination between end-member solutions; and c) pH and pCO_2 effect: strong dependence of the speciation of carbon with pH.

The saturation of a mixture also depends on the pH and pCO_2 because of the strong dependence of carbonate system with pH (Figure 5.1c). Thus, the CO_3^{2-} concentration will be higher under slightly basic conditions than under acidic ones for the same Ca concentration. Thus, the mixture of slightly acidic fluids will be more easily subsaturated than the mixture of more basic ones. Changes in temperature may also affect the saturation of a mixture due to the non-linear dependence of that with the mineral equilibrium constants. However in non-geothermal groundwaters, temperature variations exceeding 10ºC are not expected within the range of a few meters (the scale of the carbonate cavities) and the temperature effect becomes practically negligible (Corbella and Ayora, 2003).

The theory of carbonate undersaturation by mixing has been extensively used to interpret carbonate dissolution textures found in caves and borehole samples from coastal environments (Plummer, 1975). Reactive transport modeling exercises have demonstrated that important porosity development may occur at the salt water-fresh water mixing zone of coastal aquifers (Sanford and Konikow, 1989; Rezaei et al., 2005). Mixing of two fluids with different salinity has also been used as a hypothesis to explain deep dissolution of carbonates and the formation of hydrothermal mineral deposits (Corbella et al., 2004).

However, field evidences are not conclusive. Observation of mixing and carbonate dissolution at depth has not been possible because of technical difficulties. More accessible to observation is the seawater mixing zone in coastal aquifers where calcite undersaturation and/or calcite dissolution have been reported numerous times (Back et al., 1979; Hanshaw and Back, 1980; Back et al., 1986; Smart et al., 1988; Stoessell et al., 1989; Ng and Jones, 1995; Whitaker and Smart, 1997). Yet, dissolution in coastal environments is not always clear. Lack of undersaturation (Plummer et al., 1976; Magaritz and Luzier, 1985; Price and Herman, 1991; Wicks et al., 1995;

Pulido-Leboeuf, 2004) or lack of correlation between changes in cement type or porosity development and current or recent location of mixing zones have also been described (Maliva et al., 2001; Melim et al., 2002). Moreover, dissolution evidences admit alternative explanations. For example, sea level has oscillated tens of meters during the Pleistocene and this may have caused diluted continental water to invade and dissolve carbonate aquifers in the same area where prior or later salt water intrusion and mixing is assumed. Therefore, observation of dissolution features in the carbonated matrix is not enough to ensure that calcite dissolution is actually occurring under mixing conditions. In summary, laboratory experiments to validate the reliability of model predictions are required.

The only reported laboratory experiments of carbonate reaction by mixing saturated solutions were performed by Singurindy et al. (2004). They used a 2D flow cell filled with crushed calcite in which two extreme solutions were injected at different flow rate along two cell faces, while the other two allowed mixed solution outlet. End-member solutions were deionized water and 40g/L NaCl solution, both equilibrated with calcite at room temperature. Dissolution was evidenced to take place for input flow ratios of 30 and 50% of saline water by an increase in the measured Ca concentration in the outlet solution with respect to the inflow mixture. They observed higher dissolution for the 30%-salty mixing and results were in reasonable agreement with predictions from a relatively simple transport model. However, no quantitative relationship of subsaturation with dissolution extent was shown, due to limitations of the experiment design. Indeed, mixing subsaturation and dissolution did not occur uniformly throughout the flow cell.

In summary, neither field observations nor laboratory experiments have allowed a detailed comparison between subsaturation predictions with observations of current calcite dissolution. In this context, the objective of our work is twofold:

- To numerically test the relationship of calcite saturation and potential dissolution with the mixing proportion of two end-member solutions equilibrated with calcite.
- To compare the predictions on calcite dissolution with laboratory results from flow-through experiments with variable pCO_2.

5.1. Calcite saturation as an indicator of potential dissolution

It is assumed that the degree of subsaturation of a solution is a direct estimator of its potential for mineral dissolution. However, the discussion below reveals that this is not necessarily so. We have developed a simple calculation consisting on mixing two calcite-saturated end-member solutions at different mixing proportions, and allow the dissolution of calcite to occur towards the equilibrium. These simulations were performed with PHREEQC and the Pitzer ion-ion interaction

coefficients (Parkhurst and Appelo, 2006). The two end-member solutions (Table 5.1) were selected to reproduce a plausible seawater intrusion mixing zone in natural coastal aquifers (Rezaei et al., 2005). It should be noted that, although subsaturation is produced also for mixing with seawater, in this study the seawater was replaced by a solution with higher ionic strength in order to enhance the salinity effect and therefore subsaturation. The composition of the salty solution was pure NaCl to reduce ion-pair effects and complexity on results interpretation.

Table 5.1: Input end-member solutions used in the experiments

Name	pH	Ca tot (m)	Na tot (m)	Cl tot (m)	pCO2	SI calcite	I
Fresh solution	8.30	5.29×10^{-4}	0.0	0.0	3.5	0.0	0.002
Salty solution	7.38	3.70×10^{-3}	1.0	1.0	2.0	0.0	1.010

Simulation results are presented in terms of variation of the calcite saturation and dissolved calcite up to equilibrium with respect to the mixing ratio (Figure 5.2). It is shown that the maximum dissolution is calculated to occur for a mixing ratio of about 50% while the higher subsaturation is obtained for a mixing ratio of 15-20%. The overall dissolution reaction considered for calcite is expressed as:

$$CaCO_3 \rightarrow Ca^{2+} + CO_3^{2-} \quad (5.1)$$

Therefore, in order to gain some insight into this paradox, we computed the activities of the species controlling dissolution, Ca^{2+} and CO_3^{2-}, for both input and equilibrium solutions, in steps of 5% mixing ratios. Results are shown in Figure 5.3a. Note that calcium activities are about two orders of magnitude larger than those of carbonate. The different input mixtures show very similar CO_3^{2-} activity and a wide range of Ca^{2+} activities. Calcite subsaturation increases towards the fresh end-member solution because of the sharp decrease of activity coefficients in response to increases in salinity near the freshwater end member (Figure 5.3b).

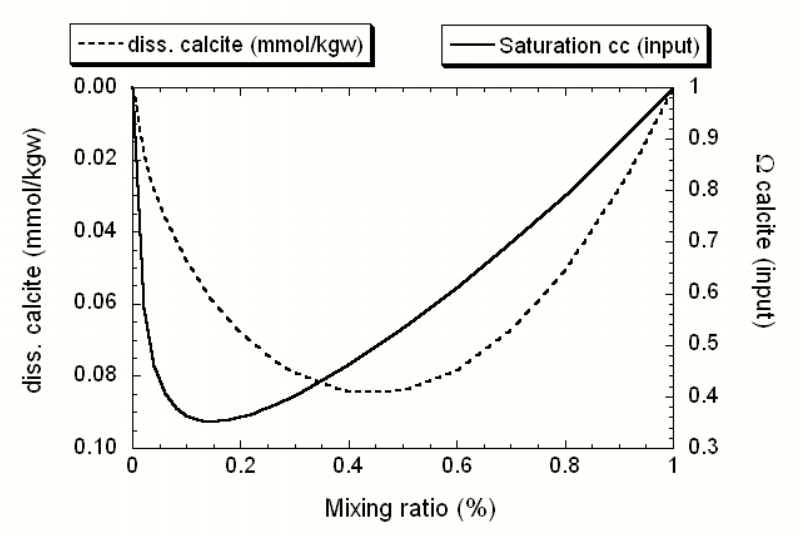

Figure 5.2: Computed saturation state and dissolved calcite after reaction to equilibrium for mixtures of the two solutions described in Table 5.1. Salinity increases to the right.

Concentrations (and thus activities) of calcium and carbonate in solution increase when calcite dissolves congruently. The moderate value of pH causes most dissolved carbonate to become bicarbonate (this is why the activity of CO_3^{2-} is two orders of magnitude lower than that of Ca). Moreover, the difference in pH between end members (pH fresh= 8.30; pH salty= 7.38; see Table 5.1) promote higher bicarbonate/carbonate ratio in solution, and more calcite needs to be dissolved to restore the CO_3^{2-} activity. As shown in Figure 5.3a, dissolution of calcite increases from 0 to 15%-salty mixtures because of the decrease in saturation state. For mixtures with more saline water, subsaturation begins to decrease with salinity increase. Yet, total dissolution still increases, as evidenced by the higher value of the x-component of the vector driving to saturation in Figure 5.3a. This component measures the amount of Ca^{2+} activity required to reach equilibrium. The amount of calcite is actually measured by the increment in Ca concentration of the solution, and can be considered roughly proportional to the Ca^{2+} activity variation. Note that the activity coefficients of ions decrease with salinity and the differences between concentration of calcium in solution and its activity are also larger. For mixtures with more than 50% of saline water this effect is negligible (Figure 5.3b), the saturation state becomes smaller and less calcite is dissolved.

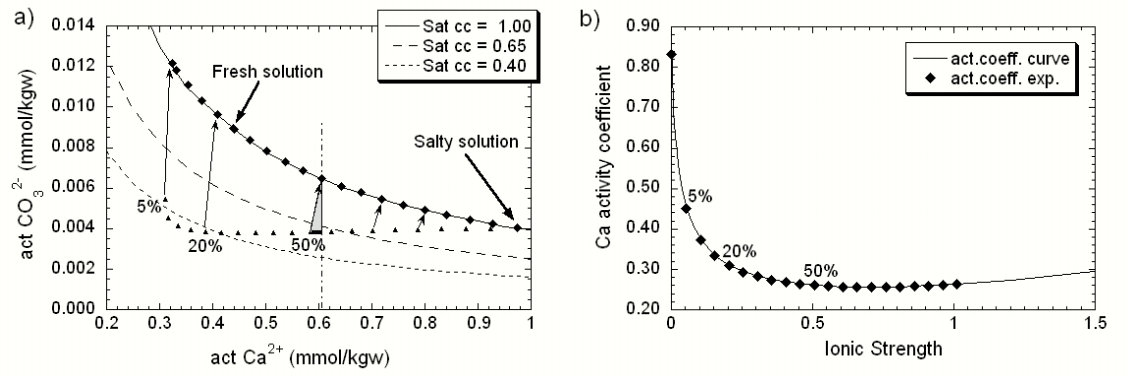

Figure 5.3: Relation of calculated activities of Ca^{2+} and CO_3^{2-} in the mixed solutions. Solutions are depicted every 5% of mixing ratio. Triangles represent the mixed input solutions and filled diamonds the mixed solutions after reaction to equilibrium. Arrows represent the evolution of the solution composition with dissolving calcite. The curves represent several calcite saturation states (Ω).

5.2. Materials and methods

5.2.1. Experimental setting

Dissolution experiments were carried out using 35 mL flow-through Lexan reactor cells (Metz and Ganor, 2001) at temperature of 25 ±1.5 ºC. Flow-through experiments allowed us to measure dissolution rate under different flow rates (i.e., residence time) and initial powder mass (i.e., water/rock ratio). Inside the cell, calcite reacted with a through-flowing fixed mixture of two end-member solutions with different salinities. Each of these extreme solutions was equilibrated with calcite and a certain pCO_2 in separate hermetic reservoirs prior to the mixing (Figure 5.4). Equilibrium with calcite was ensured by adding calcite powder (Merck, pro analysis quality, 99.0% purity) in excess into the reservoirs, and maintaining the solutions constantly stirred with a stirring magnet inside the reservoir tanks. Commercial N_2-CO_2 gas mixtures were bubbled into the reservoirs for two hours twice a day, what was found (in preliminary tests, measuring pH and Ca and Na concentration) to be enough to maintain calcite-equilibrium at the desired CO_2 pressure (see Table 5.1).

Tank solutions were pumped into a mixing stirred cell. Before entering the mixing cell, solutions were filtered through a 0.45 μm filter, thus preventing suspended calcite particles from entering the tubing system (Figure 5.4). A set of preliminary tests (not shown) were performed to show that solution reservoirs, connections and tubes (made of PVC) behaved practically impervious to CO_2 diffusion. However, the reactor cells allow some gas transfer with the laboratory atmosphere. The CO_2 in the laboratory presented a stable pressure of $10^{-3.22}$ ±10% bar over the duration of the experiments.

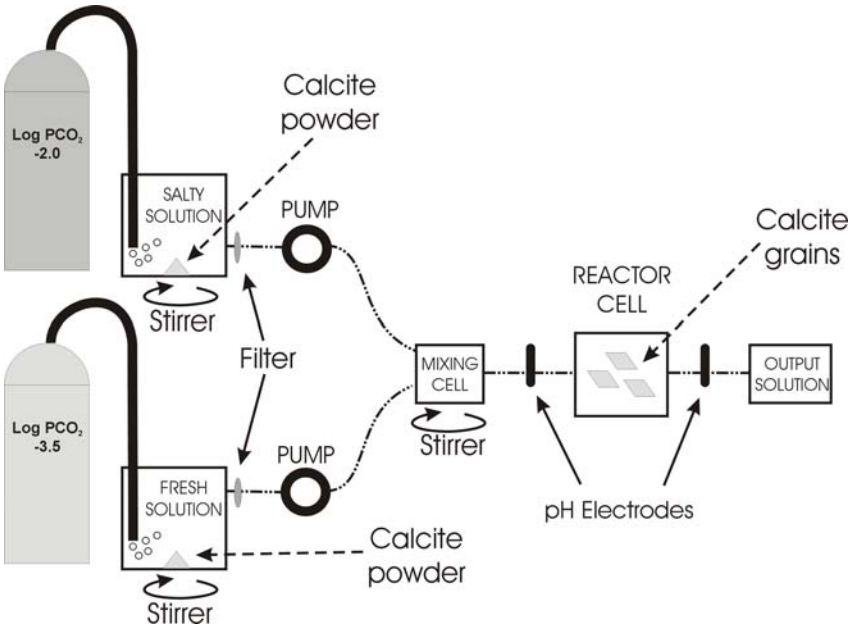

Figure 5.4: General experimental set-up showing the flow-through system used in the present study.

Stable flow rate and fixed mixing ratios were achieved combining two peristaltic pumps running at different rates and/or using pumping tubes of different diameters. Flow rate was double checked by volume-weighted output solution every 8 hours. Flow rates ranged from 8.33×10^{-7} to 1.00×10^{-5} kgw/s, with 1.66×10^{-6} kgw/s for most of the experiments (see Table 5.2 for details). pH was continuously measured in-situ upstream and downstream of the reactor cell using sealed cells with a single glass electrode (Orion #9157BN) interfaced with a computer (through a Orion 720A pH meter). These measurements correspond to mixed-input and reaction pH, respectively (Figure 5.4). The pH electrodes were maintained with 2-point calibration (standard solutions of pH 7.00 and 9.21) every 24 hours.

Experiments consisted of one or several sequential stages. When sequential stages were considered, solid was not changed but the flow rate or mixing ratios varied (Table 5.2). Experiments were run for every stage until steady input and output Ca concentrations was observed for a long enough time. Subsequently, they were stopped or the conditions modified to a new stage. The design of the experiment ensured that steady state was rapidly achieved and stages lasted no longer than 9 days. Every experiment was subjected to a pre-reaction phase (with the reactor cell not connected to the system) to allow the system to reach stable flow rate and mixing ratio before reaction occurred. One of the experiments (Exp-03_p1, Table 5.2) was stopped and the reactor cell sealed for 60 hours, behaving as batch experiment. The concentration in the cell was measured at the end of that period.

Table 5.1: Experimental conditions and results of the flow-through experiments

Experiment	**Duration** (h)	**Grain size** (mm)	**Initial mass** (g)	**Recovered mass** (%)	**Flow rate** (kgw/s)	**Mixing ratio** (%)	**Ca inp** (mmol/kgw)	**Ca out** (mmol/kgw)	**d Ca** (mmol/kgw)
Exp-01	111	125-250	0.5029	91	1.02×10^{-5}	16.7	0.878	0.893	0.015
Exp-02_b	36	125-250	0.5039	90	1.62×10^{-6}	14.4	0.952	0.974	0.022
Exp-02_c	44	125-250			5.14×10^{-6}	14.5	0.929	0.940	0.011
Exp-03_a	142	25-53	0.6053	88	1.54×10^{-6}	14.4	0.942	1.100	0.158
Exp-03_b	60	25-53			1.85×10^{-6}	12.9	0.909	1.022	0.113
Exp-03_p1	60	25-53			0.0	12.9	0.909	1.089	0.180
Exp-03_d	50	25-53			1.66×10^{-6}	13.4	0.936	1.036	0.101
Exp-04_a	216	25-53	0.6083	90	1.59×10^{-6}	13.9	0.919	1.011	0.092
Exp-05_a	66	25-53	0.6020	N/A	1.59×10^{-6}	49.4	1.824	1.842	0.018
Exp-05_b	48	25-53			1.54×10^{-6}	47.3	1.801	1.841	0.040
Exp-06	165	25-53	0.6027	89	1.57×10^{-6}	20.7	1.108	1.167	0.060
Exp-07_b	107	25-53	0.6003	94	1.55×10^{-6}	21.2	1.153	1.196	0.043
Exp-07_c	97	25-53			1.59×10^{-6}	40.7	1.680	1.708	0.027
Exp-08_a	144	25-53	0.6019	93	1.57×10^{-6}	5.2	0.718	0.747	0.028
Exp-08_b	114	25-53			1.55×10^{-6}	7.4	0.777	0.837	0.060
Exp-08_c	114	25-53			8.20×10^{-7}	7.4	0.771	0.889	0.117

5.2.2. Solid and solution characterization

The calcite sample used in this study is a crystallized Iceland spar from a skarn deposit from Martinet (Eastern Pyrenees, Spain) containing only $CaCO_3$ (based on X-ray diffraction analysis). The crystal was ground with an agate mortar and sieved to fractions 125-250 µm and 25-53 µm. The BET initial surface area for these size fractions was 0.17 and 0.21 m^2/g, (measured using 5-point N_2 adsorption isotherms). We assume that the surface area did not change significantly during the experiments because of the small amount of calcite dissolved. Scanning Electron Microscope (SEM) photographs of the initial raw material show that the rhomboedrical shape of the calcite crystals, as well as clean surfaces and sharp edges were mostly preserved after grinding (Figure 5.5a). Most of the experiments were designed with the same grain size (25-53 µm) and initial mass of calcite (approximately 0.6 g) to facilitate comparison among the results (Table 5.2). When an experiment was stopped, the reactor was immediately dismantled and the remaining calcite powder was recovered, cleaned with ethanol and stored in a dry atmosphere. The recovered powder was then weighted and examined by SEM in order to quantify the effect of dissolution on crystal surfaces. Recovered mass of calcite represented 90 to 95% of the initial mass in all cases.

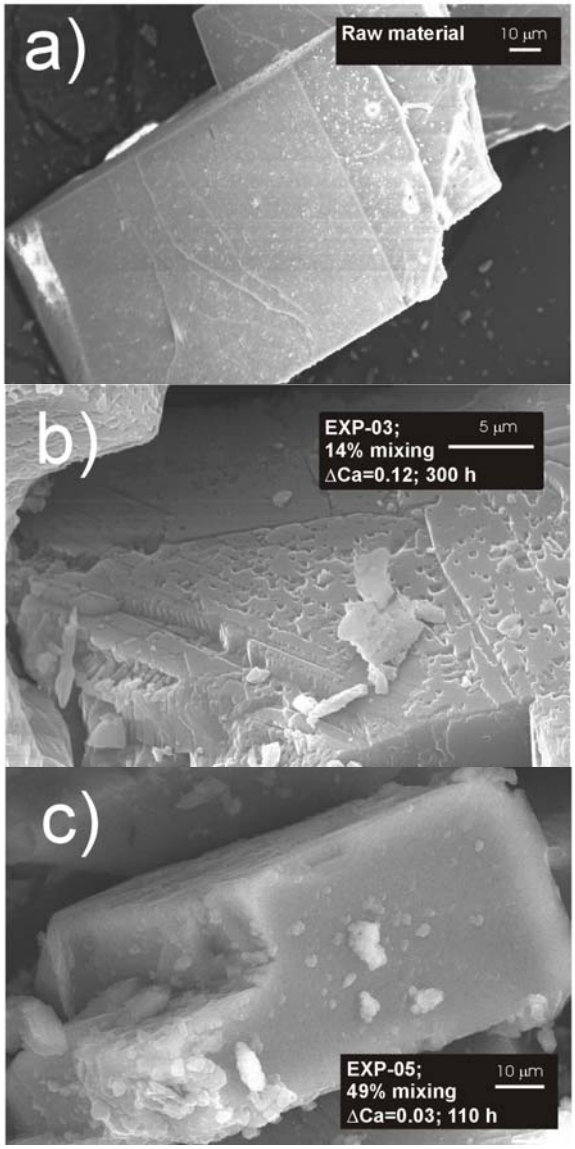

Figure 5.5: SEM microphotograph of a) raw calcite grains; b) recovered material from Exp-03 (15%), dissolution is characterized by the development of etch pits that can often grow by lateral migration or intersect, ending up forming organized linear or curvilinear trench-like chains; and d) recovered material from Exp-05 (49%), crystals appear barren on their faces but not special pattern is described. Crystal edges are clearly rounded.

All the experiments were run using the same end-member solutions, but mixed in different proportions. Fresh input solution consisted on double deionized water equilibrated with calcite and with a pCO_2 of 3.5 (that is, the standard CO_2 content in the open air atmosphere). Salty input solution was prepared equilibrating a 1 m NaCl solution (from Merck, pro analysis quality, 99.5% purity) with calcite and a pCO_2 of 2.0 (Table 5.1). Input end-member solutions were sampled and analyzed at the tanks every 24 hours over the duration of the experiments in order to check stability

of input solution conditions and detect any possible variation on the experiment conditions. Output solution was sampled every 8 hours in all the experiments. All input and output samples were analyzed for pH, and Ca and Na concentrations. Ca and Na concentration was analyzed with ICP. Analytical error on these techniques was 0.02 for pH and 3% for cations.

5.2.3. Measurement of dissolved calcite

Ca and Na concentrations in input end member and output solutions were known after analytical measurement. The mixing ratio, θ, in the ith sample was obtained from sodium concentrations assuming no interaction between sodium in solution and calcite, which leads to:

$$\theta_i = \frac{C_{Na,i-out} - C_{Na,\,fresh}}{C_{Na,salty} - C_{Na,\,fresh}} \tag{5.2}$$

where $C_{Na,\,fresh}$, $C_{Na,salty}$ and $C_{Na,i-out}$ represent the sodium concentration in the fresh end-member, the salty end-member and the ith output solutions, respectively. Ca concentration in the ith mixed-input solution, $C_{Ca,i-inp}$, is obtained from the mixing ratio as:

$$C_{Ca,i-inp} = \theta_i\, C_{Ca,salty} + \left(1-\theta_i\right) C_{Ca,\,fresh} \tag{5.3}$$

where $C_{Ca,\,fresh}$ and $C_{Ca,salty}$ represent the calcium concentration in the fresh and salty end member solutions, respectively. Dissolution of calcite for different mixing ratios was quantified from the increase of Ca in solution after reaction and from the observation of dissolution features on the crystal surfaces under SEM.

Experiments conditions were designed to get the most appropriate balance among initial mass, calcite grain size, and residence time in the reactor cell, and tested in a series of preliminary tests. Several difficulties were encountered to obtain a stable signal of pH input and output in the system. Although the pH after reaction was higher than the input for all cases, the uncertainty associated with the measurement excluded these observations to be used as an accurate measurement of the calcite saturation in the reactor cell. Further, experiment conditions were modelled with the reactive transport code RETRASO (Saaltink et al., 2004) and the Pitzer ion-ion interaction coefficients (Harvie et al, 1984) to test that calcite equilibrium was achieved in all cases. The code simulated kinetic dissolution of calcite following the dissolution rate of Arvidson et al. (2003). Thus, the output Ca concentration when the system reaches the steady state can be calculated from:

$$\frac{\partial C_{Ca,out}}{\partial t} = 0 = \frac{\left(C_{Ca,inp} - C_{Ca,out}\right)}{t_R} + kAf\left(1-\Omega\right) \tag{5.4}$$

where t_R is the residence time in the reactor cell (s), k is the calcite dissolution rate constant (2.0x10^{-6} mol/m^2/s), A is the reactive surface area (m^2/kgs), f is the solid:solution ratio in the reactor cell and Ω is the calcite saturation state of the solution. Eq 5.4 can be solved for Ω writing the output concentration as a function of Ω. This allows computing Ω as function of experimental conditions. Figure 4 displays Ω versus specific surface for a flow rate of 1.70x10^{-6} kgw/s, a 15%-salty mixing ratio and a solid:solution ratio of 0.6 g:20 mL reactor cell. The 15% mixing ratio is the one leading to the highest subsaturation. Hence, we can conclude that all the experiments reached calcite-solution equilibrium.

Experimental results are presented in terms of increase of Ca concentration during reaction (equivalent to dissolved calcite, Diss.cc., if congruent dissolution is assumed) as:

$$\text{Diss.cc.} = C_{Ca,out} - C_{Ca,inp} \tag{5.5}$$

and the associated error:

$$\delta_{Diss.cc} = \left(\delta^2_{C_{Ca,out}} + \delta^2_{C_{Ca,inpt}} \right)^{1/2} \tag{5.6}$$

where $\delta_{Diss.cc}$, $\delta_{C_{Ca,out}}$ and $\delta_{C_{Ca,inpt}}$ represent the errors associated to dissolved calcite and Ca input and output concentrations, respectively.

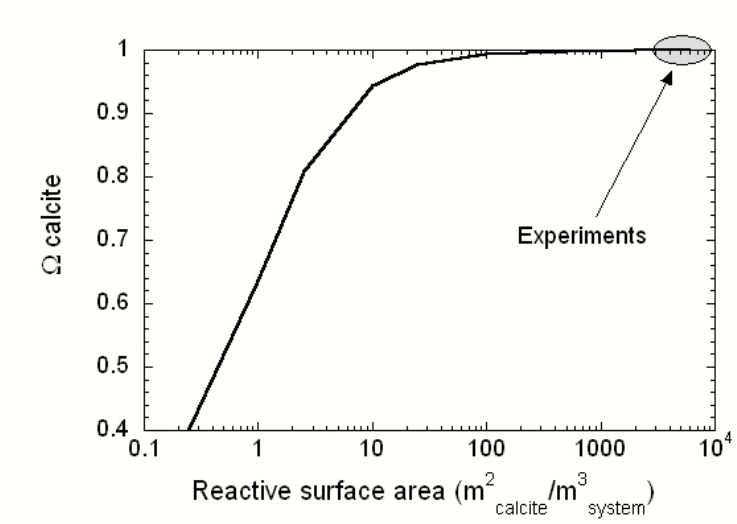

Figure 5.6: Variation of calcite saturation state of the outlet solution versus calcite reactive surface area. The values were calculated after simulation of the experimental setting with reactive transport modeling, with a mixing proportion of 15% of saline water (Table 5.1), and a total flow rate of 1.10x10^{-6} kgw/s. Note that for the reactive surface areas used, calcite equilibrium is reached in all the experiments.

5.3. Experiment results

Dissolution experiments covered the range of 0-50%-salty mixing ratios and all mixing ratios were tested at least twice. Dissolution was observed in all experiments, but its extent varies with the mixing ratio. Experimental results are compiled in Table 5.2. The time evolution of flow rate, mixing ratio and Ca concentration in two representative experiments is depicted in Figure 5.7. As shown, flow rate and mixing rate reached stability during the pre-reaction phase (negative time in Figure 5.7). Differences between input and output calcium concentration were within the analytical error in some of the experiments, but in all cases these differences were stable with time, and therefore the results were used in the discussion. It should be noted that this is a consequence of the low potential of calcite dissolution associated with mixed waters environments due to seawater intrusion in nature.

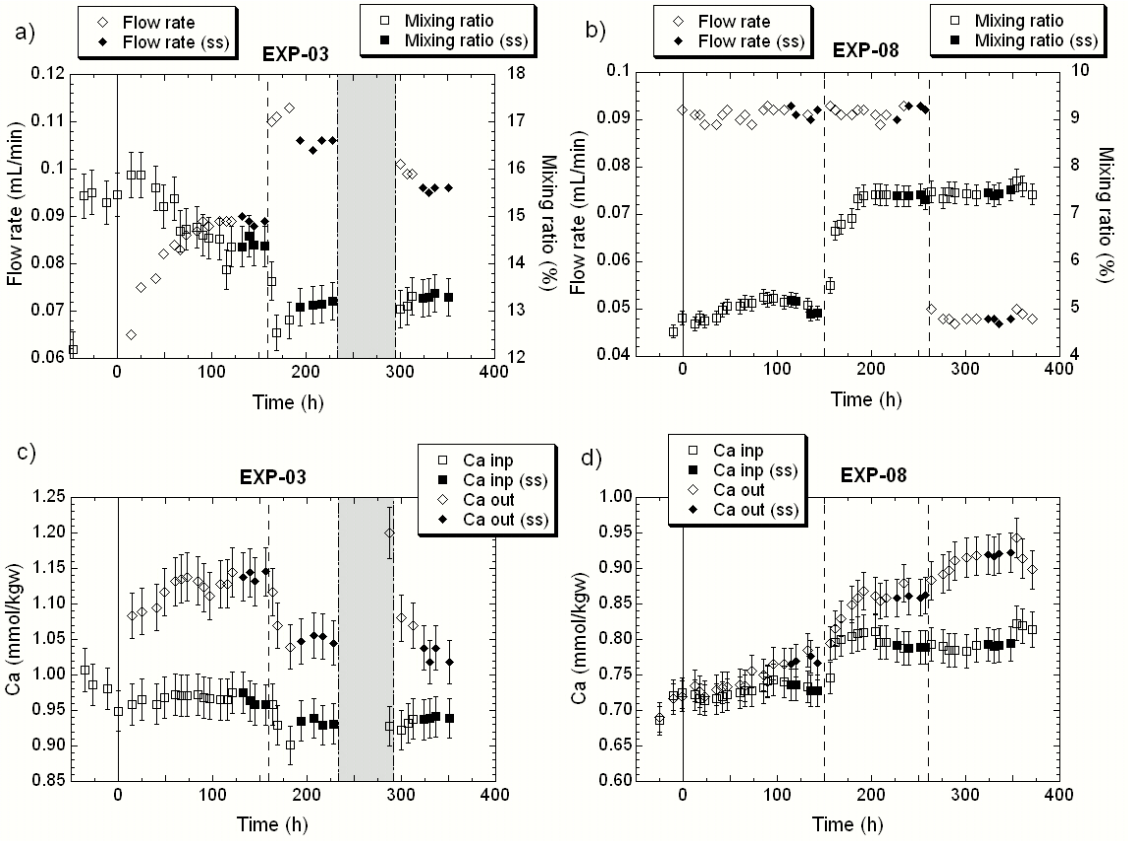

Figure 5.7: Variation in flow rate, mixing ratio, and Ca concentration input (deduced) and output (measured), as a function of time in two representative experiments. The vertical single line represents the experiment beginning and the dashed lines represent changes in experimental conditions between the different stages. Grey area indicates conditions of no flow through the reactor cell. Data used to calculate average steady state values (ss) are denoted by filled symbols (Table 5.2).

Figure 5.10 displays the measured dissolved calcite for each experiment. Results show a distribution of higher dissolution for approx. 15%-salty with an abrupt decrease of calcite dissolution for fresher and saltier mixtures in the 0-20% mixing range. For higher mixing ratios the calcite dissolution is less important. It should be noted that different amounts of dissolved calcite are observed for the similar mixing ratios, with an increase of dissolved calcite for the lower rate.

SEM microphotographs of the calcite recovered after the experiments are in agreement with the increase of Ca concentration observed. Dissolution was identified on the surface of all the recovered materials and the observation of dissolution features on crystal surfaces validated qualitatively the existence of calcite dissolution. For experiments presenting higher increase of Ca in solution dissolution were characterized by the development of etch pits that can often grow by lateral migration or intersect, ending up forming organized linear or curvilinear trench-like chains (Figure 5.5b). When less increase of Ca concentration was observed, etch pits were not found and dissolution yielded non-geometrical corrosion features that did not reproduce crystal structures. Finally, in the experiments with minor release of Ca, the calcite crystals did not show dissolution patterns in their faces, but the crystal edges were clearly rounded with respect to the initial material (Figure 5.5c). These observations are in agreement with the behaviour of calcite dissolution for different subsaturation values observed under Atomic Force Microscopy (Arvidson et al., 2003).

5.4. Discussion

The experimental setting was design to allow certain the diffusion of CO_2 between the reactor cell and the atmosphere in the laboratory. The extent of this diffusion varies in the experiments depending on the flow rate of the experiments (i.e., on the residence time in the reactor). The system then is controlled by two limit situations: a close system where the conservative mixing dissolves calcite to equilibrium with no interaction with the laboratory atmosphere, and a completely open system where the mixture dissolves calcite to equilibrium with the pCO_2 of the laboratory atmosphere. Figure 5.8 shows the variation of CO_2 content with the mixing ratio predicted for the experiment conditions. The input mixture in a close system before reaction with calcite has a higher pressure of CO_2 than the laboratory for ratios above 5% (Figure 5.8a). The opening of the system would lead to lower pressure of CO2 (arrows in Figure 5.8a) and a decrease of subsaturation. The opposite occurs for mixing ratios below 5%. The pressure of CO_2 of the solution is higher for the open system and so is the subsaturation. This effect can be observed in the calcite subsaturation of the mixtures of Figure 5.9. Results in Figure 5.9 are consistent with the discussion above and show that the calcite saturation of solutions for mixing ratios higher than 5% in the open systems increases with respect to that of the closed system. The saturation continues increasing with the mixing ratio and eventually becomes supersaturated in calcite (above 20% mixing, approx.). For

mixing ratios lower than 5%, the subsaturation in the open system is higher than that of the closed system. It should be noted that, although the diffusion of CO_2 in our system modifies the pattern of the saturation dependence on mixing ratio, the maximum subsaturation predicted remains very similar in value.

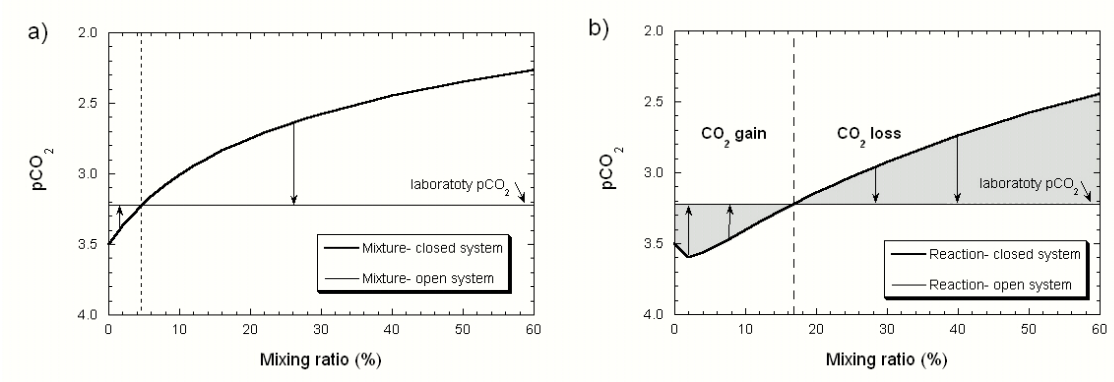

Figure 5.8: Predicted variation of pCO_2 with the mixing ratio for the close system and the system open to the laboratory atmosphere. a) Mixed solutions before reaction. b) Comparison of the solutions after reaction. The diffusion of CO_2 generates a gain or loss of CO2 in the reactor cell. Vertical dashed lines mark the breaking point of the curves and limit the ranges of mixing ratio showing opposite diffusion direction. Arrows indicate the way of change from closed to open system in both figures.

If we compare now the variation of CO_2 pressure of the mixtures after calcite dissolution to equilibrium (Figure 5.8b), for the closed and open systems, we can also differentiate to ranges of mixing ratios with a distinctive behaviour. For mixing ratios lower 17% the reactor gains CO_2 during the diffusion with the laboratory atmosphere. This increase in CO_2 will promote further dissolution of calcite and for this range of mixing ratios the dissolution of calcite will increase with the diffusion of CO_2, as shown in Figure 5.10. The process is limited by the CO_2 content existing in the laboratory, i.e., CO_2 pressure in the reactor could never be higher than $10^{-3.22}$ ±10% bar. The grey areas in Figure 5.10 represent the potential calcite dissolution under the experiment conditions. This limits the areas between the curves of calcite equilibrium for closed and open system.

In the other hand, for mixing ratios higher than 17% the diffusion decreases the CO_2 pressure in the reactor cell and the extent of calcite dissolution drops. Figure 5.10 shows that the predicted dissolution of calcite decreases sharply for ratios above 17% and eventually leads to precipitation conditions for ratios above 20%. It must be noted that the ranges of distinctive behaviour recognized for the input mixtures before reaction (Figure 5.8a) and the reaction mixtures (Figure 5.8b) have different limiting ratio (5% and 17%, respectively). This point out again the differences

the lack of correlation of the maximum subsaturation and actual calcite dissolution in these systems: the input mixtures gives and indication of the calcite subsaturation and the reaction mixtures that of the calcite dissolution.

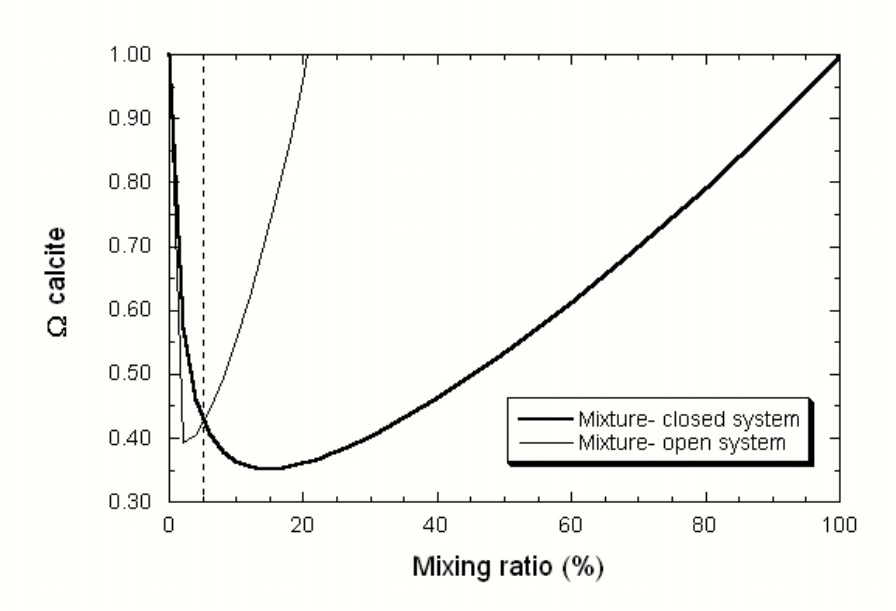

Figure 5.9: Calculated calcite saturation with respect to the mixing ratio. Lines represent values for the conservative mixing (close system) and mixing equilibrated with the CO_2 in the laboratory (open system).

Figure 5.10 also shows the amount of calcite dissolved at the experiments. It is clear that all the experimental results plot in the grey area of potential calcite dissolution. In a closer look over the results, we can group the experiments based on their residence time in the reactor. We can distinguish three groups: the experiments run with a intermediate residence time of 5.7 h (flow rate around 1.7×10^{-6} kgw/s), and the ones with higher and lower residence time. The residence time of a particular experiment has the key for limiting the extension of the CO_2 diffusion, and therefore the total dissolved calcite will vary for similar experiment conditions. Thus, two experiments run with similar mixing ratios but with different flow rate would have different CO_2 diffusion and thus dissolving a different amount of calcite.

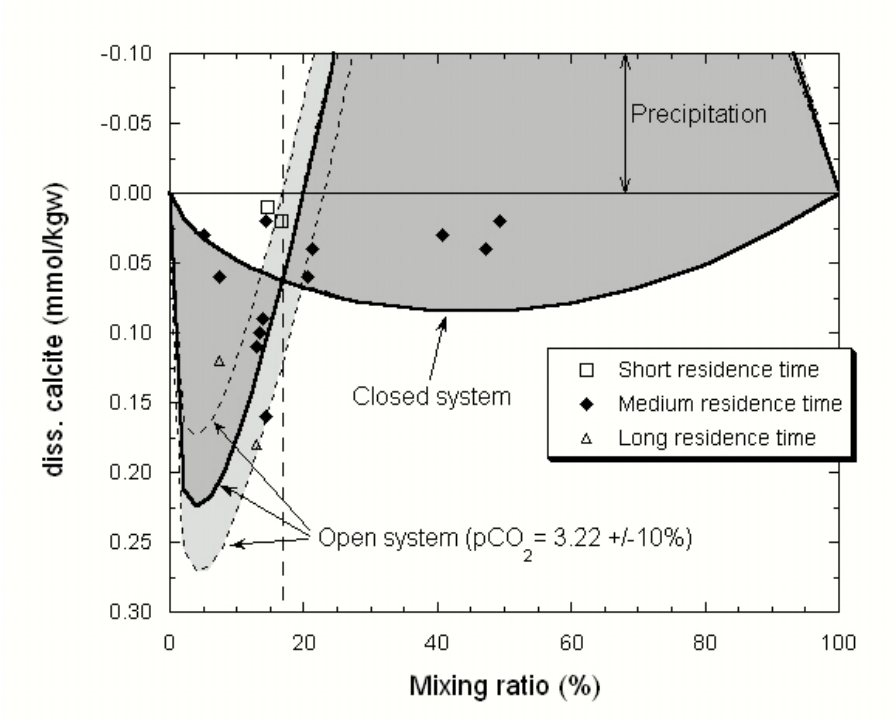

Figure 5.10: Comparison of experimental data and simulated values for dissolved calcite. Lines represent the dissolved calcite predicted for dissolution at equilibrium, for a closed system and a system open to the laboratory atmosphere of $10^{-3.22}$ bar. Note than the 10% error associated with the value is marked by the curves for $10^{-3.18}$ and $10^{-3.27}$. Grey areas represent the possible experimental calcite dissolution. Vertical dashed line limits the ranges of mixing ratios with gain (below 17%) and loss (above 17%) of CO_2 in the reactor due to CO_2 diffusion. Salinity increases to the right.

It should be noted the high sensitivity of the calcite dissolution with the small variations of the CO_2 at the reaction place. For example, as shown by the calculated curves, a variation of only 10% on the pressure of CO2 in solution may lead to significant difference on the maximum dissolution at a particular mixing ratio. This issue puts serious limits to know the actual dissolution of calcite considering the difficulties to characterize the actual P_{CO2} at depth.

5.5. Conclusions

The simulation of mixing waters of different salinities and pCO_2 but at equilibrium with calcite reveals that the variation of the saturation of the mineral is not always a good indicator of the real potential for calcite dissolution of a mixture. It is demonstrated that the maximum subsaturation is expected to occur for mixing ratios of about 15%-salty, while the expected dissolved calcite reaches its maximum for 50% of mixing. This apparent inconsistency can be explained by the strong influence of the pH in the carbonate speciation, the relative lower activity of CO_3^{2-} compared to that

of Ca^{2+} in solution, and the dependency of the activity coefficients with the mixing ration (i.e., with the salinity variation). Therefore, the capacity of a certain mixture to dissolve calcite should be addressed in terms of calcite dissolution, rather than on the variation of calcite saturation with the mixing ratio as done in previous literature. This finding is particularly puzzling when compared with the transport results of (Chapter 6), who found that transport conditions may drive maximum dissolution towards the freshwater end. When the two results are put together, it is apparent that quantitative predictions of calcite dissolution require a reactive transport modeling.

This situation is tested through a series of flow-through experiments carried out with end-members of different salinity and pCO_2, and for different flow rates and a range of mixing ratios of 0-50%-salty. Diffusion of CO_2 at the reactor cell allows to test the effect that minor variations of CO_2 in the aquifer may have in the potential for dissolution of mixing waters. The dissolution of calcite was confirmed by direct observation of the crystal surfaces, and quantified by measuring the release of Ca.

Experiments clearly show a strong dependency of the dissolution with the mixing ratio and with minor variations of CO_2 at the reaction place. Experiments results are consistent with the calcite dissolution predicted from obtained with the geochemical modelling, and confirm the discrepancy between saturation and actual dissolution patterns.

Aquifers often present unallocated buckets of organic matter that may alter the geochemistry of groundwater (and specially the CO_2 pressure). However, P_{CO2} measurements in the field are difficult to obtain and often generate the highest uncertainties when modelling seawater intrusion field cases. Therefore, the high sensitivity demonstrated by the geochemical model to the CO_2 content in solution can explain the variety and “contradictory” field observations (dissolution vs. lack of dissolution), and is of great importance for future modelling of natural systems, especially when the modelling results are scaled into geological time.